Near field read-out of a 50 GB first-surface disk with NA=1.9 and a proposal for a cover-layer incident, dual-layer near field system

F. Zijp*, M.B. van der Mark, J.I. Lee, C.A. Verschuren, B.H.W. Hendriks, M.L.M. Balistreri, H.P. Urbach, M.A.H. van der Aa, A.V. Padiy
Philips Research, Prof. Holstlaan 4, WY-32, 5656 AA Eindhoven, The Netherlands
** Phone: +31 40 2742629, Fax: +31 40 2744927, E-mail: Ferry.Zijp@philips.com*

Abstract: We present read-out results of a 50 GB disk with a blue laser and a NA=1.9 Solid Immersion Lens in a conventional focus and tracking actuator. Furthermore, we show a light path and a disk design that enable cover-layer incident near field recording on dual-layer disks with a capacity of 300 GB on a double-sided disk.

1. Introduction

In this paper we report on our progress in developing a system for a home server application that will ultimately store over 300 GB on a removable double-sided CD-size disk in a sealed cartridge. To achieve this target we combine near field optics with advanced channel coding and bit detection techniques as reported at ODS2004 [1, 2]. In our system we use a Solid Immersion Lens (SIL) in a biaxial actuator with a digital servo system for maintaining a constant air gap between the SIL and a very flat disk, an approach similar to the one reported by Shinoda et al. [3] and Ishimoto et al. [4]. Considering just the optics of such a system, there are two options to achieve our target capacity of 300 GB on a CD size disk. The first option employs a very high Numerical Aperture NA ≈ 1.9 with a first-surface optical disk. The second option is based on a smaller NA ≈ 1.5 but uses a dual-layer disk with a protective cover-layer. In this paper we report on both approaches. In the first part of this paper we report on our progress in designing and testing a near field optical system with a blue laser and a NA=1.9 lens in a conventional biaxial actuator and a first-surface optical disk. We report on results in making NA=1.9 lenses, the performance of our air gap servo system and we comment on the robustness of the system. Finally we present results of near field read-out of a 50 GB disk with our NA=1.9 lens and a study on the spot size and gap induced aberrations in near field systems. In the second part of this paper, we propose a 2-element lens and a disk design for cover-layer incident near field recording on dual-layer disks with NA=1.5. We discuss the problem of spherical aberration compensation for near field dual-layer disks and we estimate the minimum spacer layer thickness that can be allowed in a near field dual-layer optical disk system.

2. Design and manufacturing of a NA=1.9 objective lens for first-surface disk read-out

We have designed and manufactured NA=1.9 objective lenses for 405 nm light that consist of a NA_0 = 0.45 plano-aspherical lens and a super-hemispherical aplanatic SIL made of LaSF35 glass with n=2.09 (Fig. 1a) and a diameter of only 1.0 mm. The aplanatic SIL is a well-known special design solution in which light is focused free of wave front aberration inside the super-hemispherical SIL if the geometry satisfies the aplanatic conditions sketched in Fig. 1b, where R is the SIL radius. The aplantic condition requires that the SIL thickness be exactly $t_{SIL}=R(1+1/n)$ while the SIL is positioned on axis at a distance nR away from the focal point in air of the aspherical lens. This super-hemispherical SIL increases the effective NA to $NA = n^2NA_0$ inside the SIL. The corresponding spot size improvement is also found in the air gap between the SIL and the disk as long as the air gap is smaller than the decay distance of the evanescent wave vectors in the air gap. The evanescent waves in the air gap decay within a fraction of the wavelength which means that the air gap should be kept constant within a few tens of nanometers at all times during read-out and writing. In order to obtain sufficiently large margins for disk tilt with respect to the flat side of the SIL at such a small air gap, the SIL has a conical shape with a small 40 μm diameter flat tip (Fig. 1c) in which the laser beam is focused. Because of the large angles of the marginal rays at the spherical air-SIL interface, an anti-reflection coating has been applied on the SIL to reduce the reflection of the marginal rays at the air-SIL interface from 40% without coating to 5% with coating. The objective lens is mounted in a conventional Philips DVD actuator for air gap control and tracking, see Fig. 1d.

Optical Data Storage 2004, edited by B. V. K. Vijaya Kumar, Hiromichi Kobori,
Proceedings of SPIE Vol. 5380 (SPIE, Bellingham, WA, 2004)
0277-786X/04/$15 · doi: 10.1117/12.562376

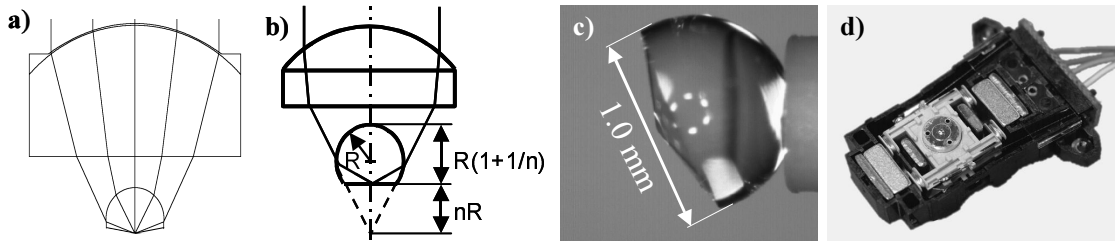

Figure 1 a) *Design principle of a NF objective with a super-hemispherical SIL,* ***b)*** *Actual NA=1.9 design,* ***c)*** *Photograph of the SIL,* ***d)*** *Complete DVD actuator with NF objective.*

The aplanatic SIL has quite good tolerances with respect to positioning relative to the aspherical lens and field, the tolerance on SIL thickness however is severe. If we accept a spherical aberration limit of 15 mλ RMS in the SIL manufacturing process than the SIL thickness tolerance is only 0.2 μm. Taking into account the tolerances on the SIL diameter and refractive index we found that we could not achieve this 0.2 μm tolerance for this type of shape and material with the current state of the art manufacturing (grinding and polishing) alone. To solve this problem we used interferometric wavefront analysis in combination with a Focused Ion Beam (FIB) milling process. The FIB milling process was used to fine-tune the SIL thickness in order to obtain less than 15 mλ RMS spherical aberration for the assembled objective lens. This was checked with a phase stepped Twyman Green interferometer. We also use feedback from interferometric wavefront analysis to correctly mount the lens elements in the objective lens holder.

In the optimisation process we use results from ray tracing analysis of our lens design to calculate the spherical aberration as a function of the SIL thickness. The result is shown in Fig. 2a in which the Zernike spherical aberration (denoted A_{40}) is plotted as a function of the SIL thickness error for NA=1.8. The reason for testing at NA=1.8 is historical, later we started making lenses with a clear aperture up to NA=1.9. In the analysis it is assumed that the SIL is made of LaSF35 glass with n=2.086 at a wavelength of 405 nm and that the SIL has a radius R = 0.5 mm. Our SIL thickness optimisation process based on FIB milling and interferometric testing is done in steps listed below.

- A flat side is made to LaSF35 SIL spheres by polishing to a thickness that is slightly thicker (typically 4 microns) than the aplanatic condition on SIL thickness, taking into account all relevant tolerances of the spheres and the polishing process.
- The SIL is mounted in a lens holder, and a thin conducting film (typically 50 nm aluminum) is deposited on the conical side of the SIL. A conducting layer is required during the FIB milling and imaging process to prevent building up of charge on the SIL surface.
- The aspherical lens is put in the lens holder after which the assembled lens is positioned in a Twyman-Green interferometer to measure the even Zernike aberration polynomials. The amount of measured defocus is checked to fine-tune the distance between both lens elements and focus the light on the aluminum film on the flat tip at the apex of the conical shape of the SIL. This effectively makes a cat's eye geometry in which the cat's eye reflector is formed by the tip at the apex of the SIL itself.
- The measured spherical aberration over a pupil corresponding to NA=1.8 is used to derive the SIL thickness error using the curve in Fig. 2a.
- The assembled lens is removed from the interferometer and put in a Focused Ion Beam (FIB) scanner, both in order to image the SIL tip using the secondary electrons detector as well as to locally remove the aluminum and a few microns of the glass SIL tip. The FIB can remove extremely thin layers of material by bombarding the material with gallium ions. The resulting SIL tip is extremely flat and smooth.
- The assembled lens is put back in the interferometer to measure the Zernike spherical aberration. If the spherical aberration tolerance is not met another FIB milling step is performed.

Note that FIB milling processes are already being used in mass production of read-write heads for magnetic hard disk drives to reduce the size of magnetic pole tips (a process known as "pole trimming").

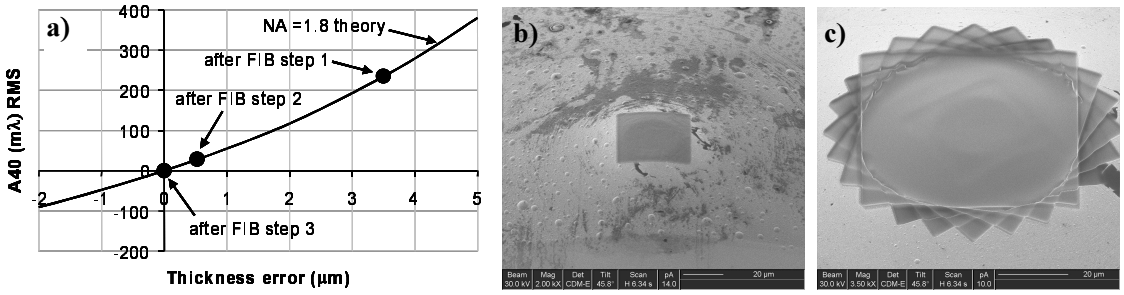

Figure 2 a) *Zernike spherical aberration (denoted A_{40}) is shown as a function of the SIL thickness error for NA=1.8. The solid dots give the measured A_{40} after the first, second and final FIB milling step.* ***b)*** *FIB image of the LaSF35 SIL tip after the first FIB milling step in which a square of aluminum has been removed;* ***c)*** *Same, after the final FIB milling step of 7 rotated squares.*

In Fig 2a, the measured spherical aberration is indicated after the first FIB milling step (first removal of a 40x40 micron square of the aluminum). The corresponding FIB image is shown in Fig. 2b and its cat's eye interferogram is shown in Fig. 3a. Note that the interferogram clearly shows an inner circle for which the NA<1. The brighter outer ring corresponds to total internal reflection for 1<NA<1.9. Further indicated in Fig 2a are the spherical aberration after a second FIB milling step (removal of several microns of glass), corresponding to the interferogram in Fig. 3b and after a third FIB milling step by which the final thickness is trimmed such that the spherical aberration is zero. The final geometry of the SIL tip after the third FIB milling step is shown in Fig. 2c. The interferogram in Fig. 3c shows straight horizontal fringes giving proof of both small defocus and spherical aberration in the final result. As mentioned above, the even Zernike aberration polynomials have been measured using a cat's eye interferometric measurement (Fig. 3a-c) which does not allow measurement of the anti-symmetric Zernike aberrations. These anti-symmetric aberrations have been checked with a near field Ronchi test on a 200 nm pitch reflective grating (Fig. 3d-e). Based on these measurements, we find a typical total residual wavefront error after assembly better than 40 mλ RMS. The spherical aberration is typically better than 15 mλ RMS, which shows that the SIL thickness tolerance was met. During the manufacturing process and interferometric measurements described above we actually measure the optical thickness and quality of the near field objective lens as a whole. This allows us to correct the SIL thickness to a value that is optimum with respect to thickness, diameter and refractive index variations in a batch of polished SIL lenses. On top of that, the spherical aberration that may be present in the aspherical focusing lens element is also compensated for. We should also point out that all interferometric wavefront analysis was compensated for a spurious polarization induced astigmatic effect. We found that polarization of the light appears to induce a large amount of astigmatism in the interferometric cat's eye measurement that is not representative of the lens quality. In accordance with theory [5], we found that this spurious effect originates from the (phase) difference in the internal reflection of the S- and P-polarized components of the light at the flat SIL tip. This implies, that for correct wavefront analysis, two interferometric measurements with linearly polarized light are required with the polarization rotated by 90° between both measurements. All our interferometric measurements were corrected this way.

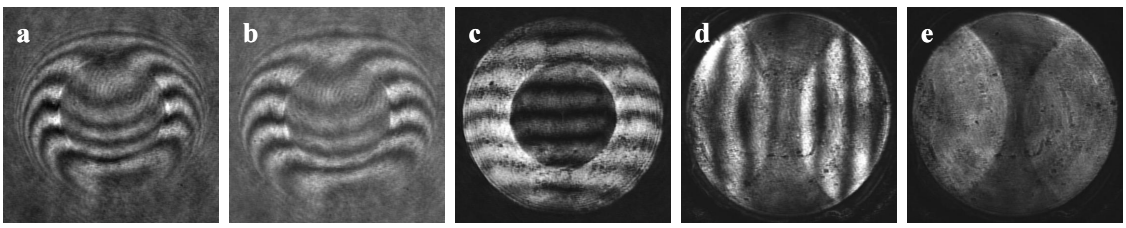

Figure 3 a) *Interferogram of the aberrations of an assembled objective lens after FIB milling step 1,* ***b)*** *Interferogram after step 2,* ***c)*** *Interferogram of the final result after step 3,* ***d)*** *near field Ronchi test on a 200 nm pitch grating with defocus added to show fringe straightness,* ***e)*** *Ronchi test without defocus.*

3. Near field optical system for read-out of first-surface ROM disks

A schematic diagram of our experimental near field player set-up is shown in Fig. 4. For air gap control and tracking we use a conventional Philips DVD actuator in which we mounted the NA=1.9 lens described in Section 2. Read-out experiments have been performed on a 50 GB silicon disk, mastered by Electron Beam Recording. All experiments were done in regular atmosphere without the use of special means to clean the air or to prevent dust particles or other contamination on the disk.

The set-up consists of a main branch comprising a blue-violet laser, collimator lens, beam shaping optics, two beamsplitters and a telescope for focus adjustment of the NA=1.9 lens. The left side branch in the figure contains a photodiode for detection of the RF central aperture signal that contains the data information and is polarized parallel to the main beam ("RF // pol."). In the same branch a split detector is positioned to generate a push-pull tracking error signal. Moreover, a CCD camera is included to observe the irradiance pattern at the exit pupil. The half-wave plate is used to control the amount of light that the Polarizing Beam Splitter (PBS) splits and directs towards the RF detector and the push pull detector, respectively. The second branch on the right side is used to generate the error signal for air gap control. In near field optical disk systems, the SIL lens needs to be positioned within the evanescent decay distance from the disk. In our set-up the SIL to disk distance is typically 25 nm. To allow air gap control with a mechanical actuator at such small distances, a suitable error signal is required. As demonstrated by Zijp and Martynov [6] and Ishimoto [4] a linear signal that is suitable as a gap error signal (GES) can be obtained from the reflected light with a polarization state perpendicular to that of the main beam that is focused on the disk. A significant fraction of the light becomes elliptically polarized after reflection at the SIL-air-disk interfaces: this effect creates the well-known Maltese cross when the reflected light is observed through crossed polarizers. By integrating all the light of this Maltese cross using polarizing optics and a single photo detector, the "RF ⊥ pol." signal is obtained. The GES is generated from the low-frequency part (DC to 30 kHz) of this "RF ⊥ pol." signal. In Fig. 5 we show the calculated reflection curves for the parallel (//) polarization, the perpendicular (⊥) polarization and the sum (total) as a function of the air gap. To make accurate measurements of the air gap width, we calibrated the GES versus the air gap. For this calibration we used the periodic oscillations that are present in the CA signal during the approach of the disk by the lens from an initially very large air gap. These oscillations are exactly half a wavelength apart and are due to Fabry-Perot-like interference between the propagating rays in the air gap. By observing the GES and the CA at the same time a very accurate calibration of the GES versus air gap curve can be made. We estimate that the error on the measurement of the gap width based on the calibrated GES is smaller than 10 %.

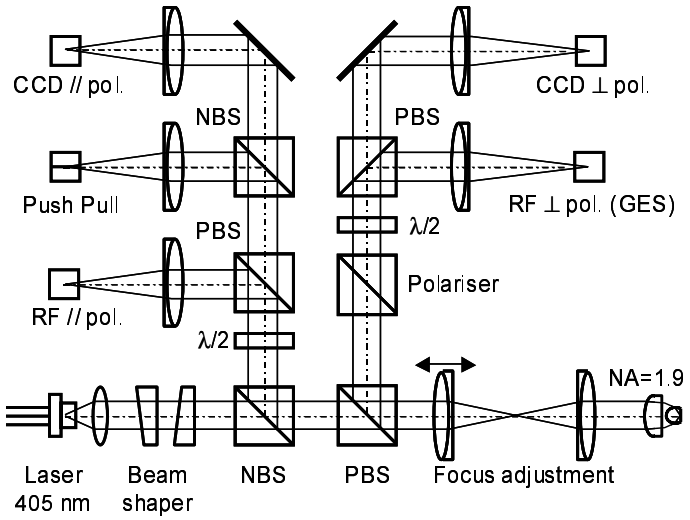

Figure 4 *Schematic of the near field player set-up (PBS = polarizing beam splitter; NBS = non-polarizing beam splitter, λ/2 = half-wave plate).*

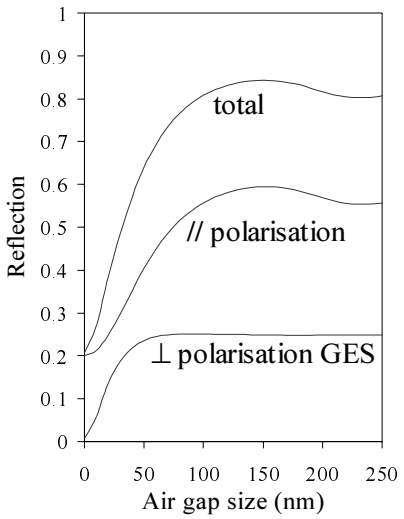

Figure 5 *Calculated reflection on a flat Si disk for the // polarization and the ⊥ polarization from which the GES is derived.*

3.1 Digital air gap servo system

As can be seen in Fig. 5, the GES signal indicates SIL-to-disk distances from 0 to about 50 nm and is constant beyond 50 nm. Therefore the air gap servo system can start its closed-loop operation only when the air gap is less than 50 nm. Because of this, the overshoot that can occur when the servo system is switched into the closed-loop operation, should significantly smaller than 50 nm to avoid lens-disk collisions. The air gap servo system we developed consists of three control modes that are switched from one to another depending on the operating condition. The system starts with an open loop approach from an initial far field position to a position where the GES becomes available. When the GES drops below a predefined threshold, the gap servo system starts a closed loop operation. To avoid a collision of the lens with the disk at this transition, the gap control reference is not set to its final value but is given a smooth reference trajectory towards the final value. This mode is called 'hand-over' control and it allows a fast and smooth switching from the open loop approach into the final closed loop air gap control. Finally, when the lens reaches the gap reference, a high-gain PID control system takes over the control. The PID controller is designed to keep the residual gap error within 2 nm at a maximum disk run-out of 10 μm at 1200 rpm rotation speed.

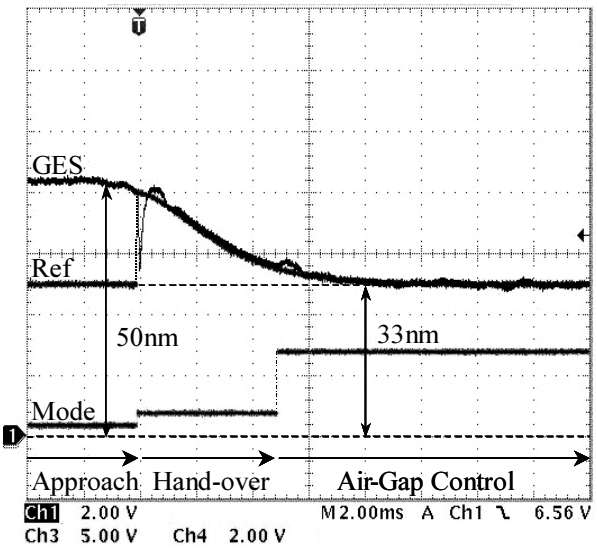

Figure 6 *Gap servo response during the pull-in stage.*

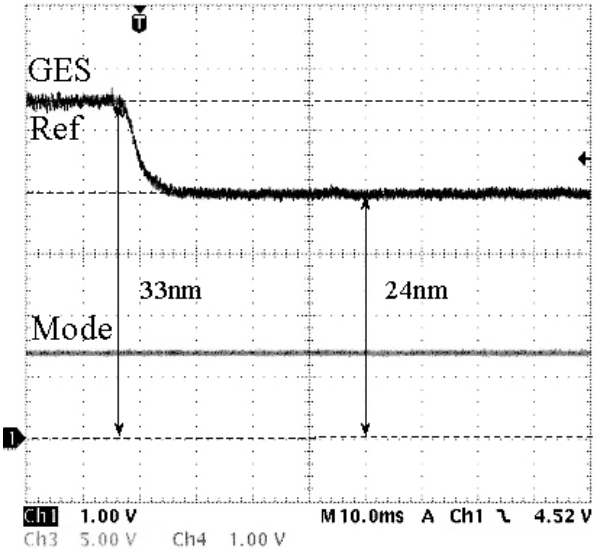

Figure 7 *Transient response of the gap servo system during a jump from a 33 nm to a 24 nm gap.*

The controller has been digitally implemented in dSPACE's real-time kernel at a sampling frequency of 80 kHz. In Fig. 6 the gap error signal "GES", the servo reference "Ref" and the control mode "Mode" of the air gap servo system is shown during starting of the servo system on a static disk. A very smooth pull-in is achieved from a far field lens position to a 33 nm air gap without collision with the disk. Furthermore Fig. 7 shows that, once the air gap servo is in closed-loop operation, then changing its gap to a different value can be done without overshoot at all. Finally, Fig. 8 a) shows the open-loop dynamic characteristics of the gap servo system. The measured cut-off frequency is 2.6 kHz, and the phase and gain margin is 44^{o} and –9dB, respectively. This allows the residual gap error of 2 nm against 30 μm disk run-out at 20 Hz as is shown in Fig. 8 b). At higher rotation speeds up to and above 3000 rpm (linear velocity of about 14 m/s), the air gap servo still works without collisions of the lens with the disk. However, due to the limited bandwidth and the occurrence of mechanical resonances in the silicon disk, amongst others, the residual gap error increases to approximately 14 nm, which is larger than our target specification of only 2 nm residual gap error. The problem of the mechanical resonances will be smaller when polycarbonate disks with more damping are used instead of the single crystalline silicon disk we use at present.

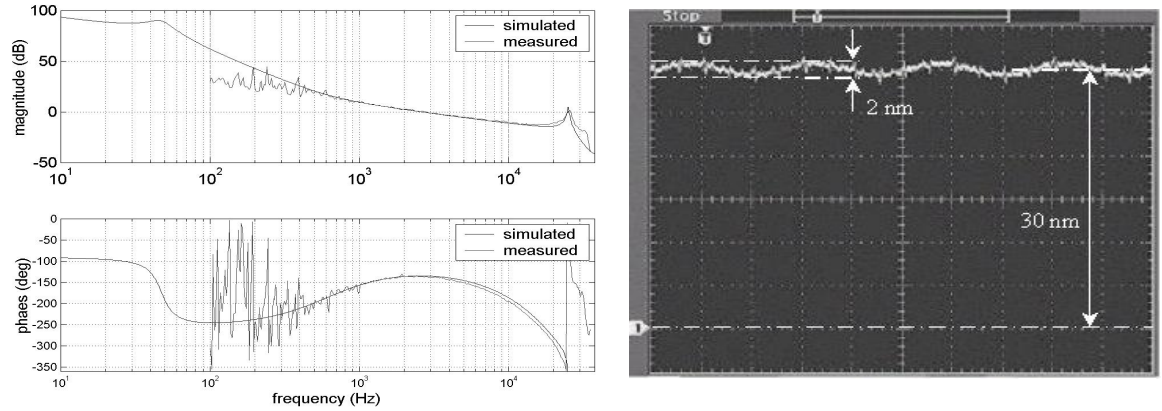

Figure 8 a) *Simulated and measured open-loop dynamic characteristics of the air gap servo system,* ***b)*** *resulting residual gap error signal against the 30μm disk run-out at the 1200rpm disk rotation speed.*

3.2 Read-out results of a first-surface 50 GB disk

In Fig. 9 we show an eye pattern of the read-out signal of a 50 GB first-surface disk. The disk material is silicon and the pits have been mastered with an Electron Beam Recorder by Sony Corporation. The channel code used on this disk is 1-7 pp with a minimum pit length of 105 nm and a track pitch of 226 nm. This density is obviously still much smaller than the potential maximum density for the NA=1.9 lens and blue laser. All experiments were done in regular atmosphere without the use of special means to clean the air or to prevent dust particles or other contamination on the disk. No protective cover layers or lubricants were used in these experiments. During this read-out experiment the air gap was kept constant at 28 nm with a residual gap error of approximately 2 nm. The linear velocity during the read-out experiment was 0.4 m/s and the read power on the disk was estimated to be 0.5 mW, however due to the fact that the lens has a NA larger than unity we could not measure the read power at the disk surface directly. During optimization of the focal position on the disk by adjusting the position of one lens of the telescope we observed that the positions for optimum RF read-out signal and for maximum radial push-pull signal are not found at the same focus position. We attribute this effect to gap induced aberrations, in particular the astigmatism that originates in the air gap due to the linear polarization of the main beam. We studied this effect also in theory as described in section 4. Due to the problem of the different positions for maximum push-pull amplitude and optimal RF we had to make a trade-off between push-pull amplitude and RF signal quality. In Fig. 9 we show the raw read-out signal eye pattern before filtering or equalization. In Fig. 10 we show the digitally sampled experimental read-out signal after digital filtering, a fixed equalizer and time base synchronization with a phase locked loop. In Fig. 11 we show the same after a limit equalizer and time base synchronization with a phase locked loop.

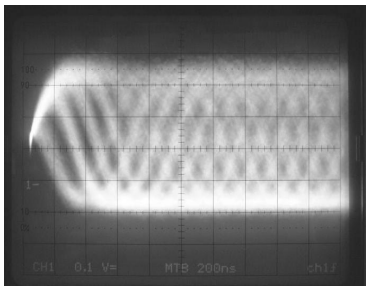

Figure 9 *Raw read-out signal eye pattern before filtering and equalization.*

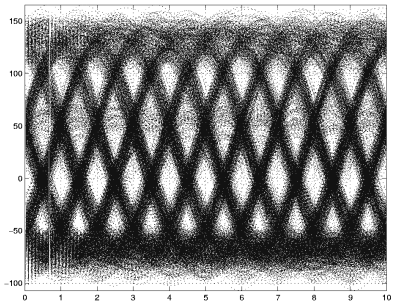

Figure 10 *Digitally sampled read-out signal eye pattern after filtering and fixed equalizer.*

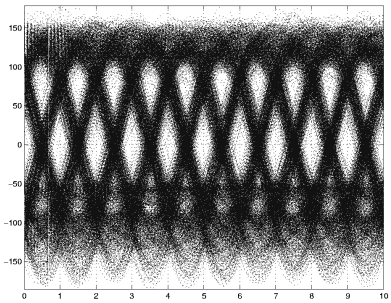

Figure 11 *Digitally sampled read-out signal eye pattern after filtering and limit equalizer.*

3.3 Robustness against dust and contamination

As mentioned before, all experiments reported in this paper have been performed in regular atmosphere in an environment with open doors to laboratory and office space. Nevertheless we observe a high degree of robustness that is genuinely surprising considering the extremely small air gap in our system. In previous work [7] we developed an optical recording system with an objective lens on a passively flying slider of the type that is found in hard disk drives. Our current actuated system with a 10 to 40 nm air gap seems to have a much better robustness against dust than our previous slider based system that was even set up in a clean room. Our experience so far seems to indicate that we have little difficulty with loose dust particles on a disk, even for an air gap as small as 10 nm. Even though we have no solid explanation for the difference in robustness between an actuator and slider based system there are some points worth noting. First of all, a slider relies on an air-bearing surface with positive and negative pressure pockets to build up air pressure on which the slider floats. We found that an important reason for failure of sliders is a built up of dust, debris and other contamination in those pockets. Our current near field system relies on active control and thus no pockets are present in which contamination can build up. It is also worth noting that the 40 μm diameter SIL tip that is closest to the disk is much smaller than the air-bearing surface of a slider. Moreover in our earlier work on sliders we found that if a slider hits the disk due to contamination in the pockets the slider itself usually survives the crash but the thin leaf spring suspension generally does not. We now observe that if the lens in our actuator collides with the disk nothing happens to the actuator. The hinges of an actuator are much more robust than the thin metal suspension one finds in hard disk drives. It is clear at this point that a lot of work still needs to be done to make near field optical recording feasible in a consumer product but the first experimental results are quite promising.

4. Gap induced aberration and near field spot size

Besides our tolerance and aberration analysis based on ray tracing for the design of our NA=1.9 lens, we also studied the wave front aberrations that are caused by focusing through a small air gap with a SIL and linear polarized light. As will be shown, these gap-induced aberrations are significant and cannot be neglected while designing a near field optical recording system. Our experimental results seem to confirm the relevance of this problem.

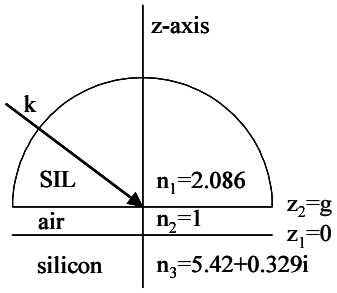

Figure 12 *Configuration of the three-layer system.*

Suppose for simplicity, we use a hemispherical rather than a super-hemispherical SIL to achieve a NA =1.9. Then the field inside the SIL consists of plane waves of which the spatial frequencies k_x, k_y fill a circular disk in frequency space of radius kn_{SIL} NA_0, where n_{SIL} is the refractive index of the SIL, k is the wavenumber in vacuum and NA_0 is the numerical aperture of the objective lens in the absence of the SIL. Hence the numerical aperture of the field inside the lens with the SIL present is $NA = n_{SIL}NA_0$. It may thus be expected that due to the hemispherical SIL the resolution is enhanced by the factor n_{SIL} . However, plane waves with wave vector $\boldsymbol{k}=(k_x, k_y, k_z)$ such that $(k_x^2 + k_y^2)^{1/2} > k$ are evanescent in air and therefore their amplitudes decrease exponentially with propagation distance z in the air gap. The size of the spot inside the disk will therefore be larger than is the case without air gap. The quality of the spot is further deteriorated by changes in phase and amplitude of the plane waves due to multiple interferences in the three-layer system consisting of the SIL, the air gap and the disk (Fig. 12). It is thus not a priori clear how small the spot inside the disk actually will be and therefore a more detailed investigation is desirable. A similar study for a slightly different configuration has been carried out by Jo et al. [8].

To study the influence of the air gap on the size of the spot in a silicon disk, we assume that a plane wave that is polarized parallel to the x-axis is focused by a diffraction-limited objective lens on a flat silicon disk. For simplicity we assume that there are no pits or grooves present on the disk. The numerical aperture of the lens is NA_0=0.911, hence vector diffraction theory [9], [10] must be applied to take the rotation of the electric field upon transmission through the lens into account. The calculation is done for the case that the image space consists entirely of the glass of which the SIL is made. In this calculation, it is furthermore assumed that the focal plane coincides with the surface of the disk (the *z=0* plane in Fig. 12). To incorporate the influence of the gap and the silicon disk on the field distribution, the plane waves are first propagated backwards from the nominal focal plane *z=0* to the interface between the SIL and the air gap (i.e. to the plane *z=g* in Fig. 12). The complex electric vector of every plane wave in the plane *z=g* is written as a linear combination of an S- and P-polarized field and these components are then multiplied by the transmission coefficient for S and P-polarization, respectively, for transmission through the interface between the SIL and the air, the air gap and the interface between the air and the silicon disk, while taking into account all multiple reflections in the air gap. For both a S- and a P-polarized plane wave, this transmission coefficient can be written as

$$t = \frac{t_{23}t_{12}\exp(ik_z^{(2)}g)}{1-r_{21}r_{23}\exp(2ik_z^{(2)}g)} \quad ,$$

where $k_z^{(j)}=(k^2 n^2_j - k^2_x - k^2_y)^{1/2}$, with n_j the refractive index of medium *j* with *j=1,2,3* referring to the SIL, the air gap and the disk, respectively. The quantities t_{ij} and r_{ij} are the Fresnel transmission and reflection coefficients for S- or P-polarization when a plane wave is incident from the side of medium *i* on the interface between two half spaces filled with medium *i* and medium *j*:

$$r_{ij} = \frac{k_z^{(i)} - k_z^{(j)}}{k_z^{(i)} + k_z^{(j)}} \quad , \text{ for S-polarization}$$

$$r_{ij} = \frac{k_z^{(i)}/n_i^2 - k_z^{(j)}/n_j^2}{k_z^{(i)}/n_i^2 + k_z^{(j)}/n_j^2} \quad , \text{ for P-polarization}$$

and with $t_{ij}=1+r_{ij}$. In the limit that the air gap becomes infinitely thin we get

$$\lim_{g\to 0} t = \frac{t_{23}t_{12}}{1-r_{21}r_{23}} = t_{13} \quad ,$$

as should be.

The amplitude and phase of *t* are shown in Fig. 13-16 for both S- and P-polarization for the laser wavelength of λ=405 nm and for several gap widths as function of $(k_x^2 + k_y^2)^{1/2}/k$. At this wavelength the refractive indices of the SIL and the silicon disk are n_1=2.086 and n_3=5.42+0.329i, respectively. It is seen that the moduli of *t* decrease for fixed gap *g* as function of $(k_x^2 + k_y^2)^{1/2}/k$ in the evanescent range $(k_x^2 + k_y^2)^{1/2}/k > 1$ where k_z^2 is purely imaginary, and as function of the gap width for fixed $(k_x^2 + k_y^2)^{1/2}/k > 1$. The modulus of *t* is a monotonically decreasing function of the $(k_x^2 + k_y^2)^{1/2}/k$ for S polarization, whereas for P polarization the modulus of *t* has a maximum at the $(k_x^2 + k_y^2)^{1/2}/k$ corresponding to the Brewster angle for the SIL to air interface. Note that for P polarization the modulus of *t* becomes larger than unity for a small interval of $(k_x^2 + k_y^2)^{1/2}/k$. Furthermore, for *g=0* and also for small *g*, the phase does not vary much as function of $(k_x^2 + k_y^2)^{1/2}/k$.

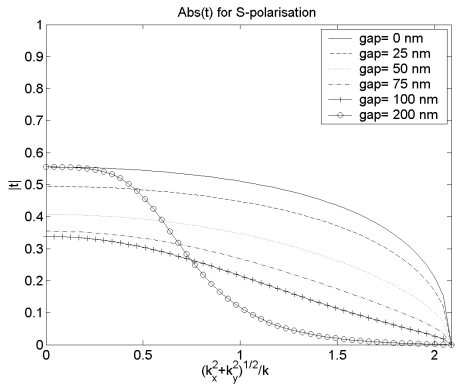

Figure 13 *Amplitude of the transmission coefficient t for S polarized light as function of* $(k_x^2 + k_y^2)^{1/2}/k$ *for the three layer system of Fig. 12.*

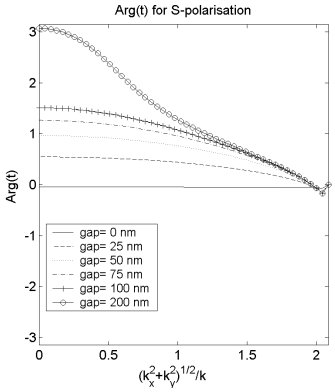

Figure 14 *Phase of the transmission coefficient t for S polarized light as function of* $(k_x^2 + k_y^2)^{1/2}/k$ *for the three layer system of Fig. 12.*

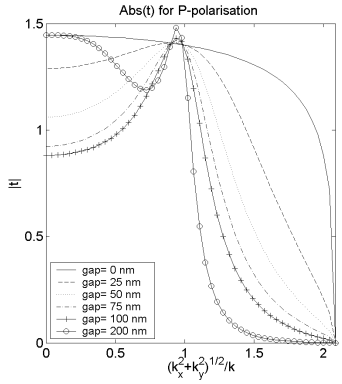

Figure 15 *Amplitude of the transmission coefficient t for P polarized light as function of* $(k_x^2 + k_y^2)^{1/2}/k$ *for the three layer system of Fig. 12.*

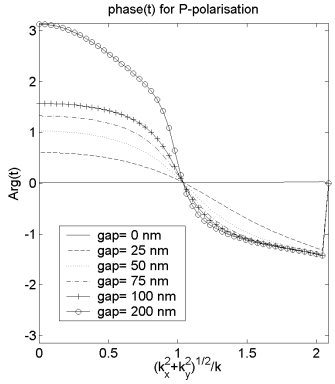

Figure 16 *Phase of the transmission coefficient t for P polarized light as function of* $(k_x^2 + k_y^2)^{1/2}/k$ *for the three layer system of Fig. 12.*

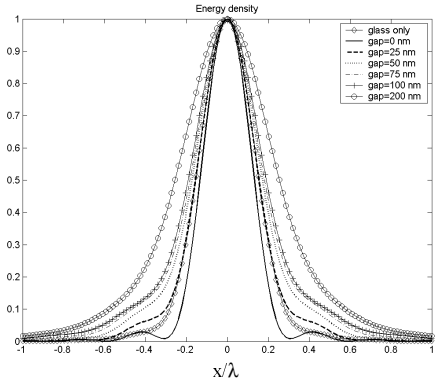

Figure 17 *Normalized cross sections of the spot along the x-axis for several air gap widths between SIL and silicon disk, and for glass only without silicon disk.*

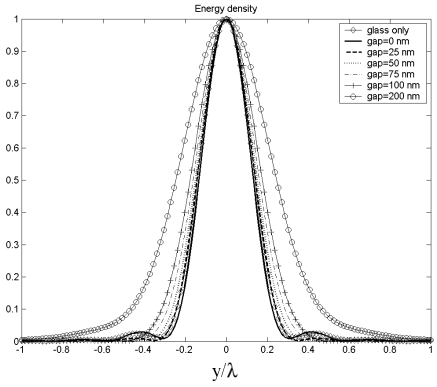

Figure 18 *Normalized cross sections of the spot along the y-axis for several air gap widths between SIL and silicon disk, and for glass only without silicon disk.*

In Fig. 17 and 18 cross sections along the x- and y-axis are shown of the normalized energy density of the spot in the surface *z=0* of the disk (considered as part of the disk) for several gap widths *g*. Also shown are the cross sections of the spot that would exist in the focal plane *z=0* when the entire image plane consists of glass of the SIL. The cross sections along the x-axis are broader than those along the y-axis, which is in agreement with the fact that the field is predominantly polarized in the x-direction. It is seen that for *g=0* the spot in the disk surface is actually smaller than the spot in the case that the image space consists of glass only, but that its side lobes are slightly more pronounced. The size of the spot quickly increases with *g* and for *g=200* nm the contributions to the spot of almost all waves that are evanescent in air are negligible and the spot therefore has the same size as when the image space consists entirely of air.

For an ideal diffraction limited lens, the plane waves that contribute to the field in the focal plane all have amplitude 1 and all have the same phase. This statement holds in fact only in the paraxial scalar theory, but still applies in good approximation to the dominant electric field component in the case of a lens of high NA. In our case the dominant electric field component is the x-component, the maximum of $|E_y|^2$ and of $|E_z|^2$ being 0.5 % and 25 %, respectively of the maximum of $|E_x|^2$. However, due to refraction at the interface with the silicon disk, which has a high refractive index, the maximum of $|E_y|^2$ and of $|E_z|^2$ just inside the disk both are of the order of 3 % of the maximum of $|E_x|^2$. We write the resolution in plane waves of the x-component in the *z=0* plane as

$$E_x(x,y,0) = \iint_{(k_x^2+k_y^2)^{1/2}<kn_1NA_0} A(k_x,k_y)\exp[i(k_x x + k_y y)]\,dk_x dk_y \quad ,$$

where the integration is over the effective numerical aperture of the lens. Write

$$A(k_x,k_y) = \left|A(k_x,k_y)\right|\exp[i\,2\pi W(k_x,k_y)] \quad ,$$

where $2\pi W$ is the argument of the complex number A. We define $a = k\,n_1\mathrm{NA}_0$ and polar coordinates ρ,φ in the unit disk:

$$k_x = a\rho\cos\varphi, \qquad k_y = a\rho\sin\varphi \quad ,$$

and we write

$$\widetilde{W}(\rho,\varphi) = W(a\rho\cos\varphi, a\rho\sin\varphi) \quad .$$

The functions W and $\widetilde{W}$ would vanish for a perfect diffraction limited lens in the paraxial theory. The deviations of W from the perfect case can therefore be considered to be caused by aberrations. By expanding $\widetilde{W}$ in terms of Zernike polynomials on the unit disk:

$$\widetilde{W}(\rho,\varphi) = \sum_{n=0}^{\infty} \sum_{\substack{m=-n \\ n-|m|\,even}} A_{nm} Z_n^m(\rho,\varphi) \quad ,$$

where

$$Z_n^m(\rho,\varphi) = \begin{cases} \sqrt{\frac{2(n+1)}{\pi}} R_n^{|m|}(\rho)\sin(m\varphi), & \text{if m} < 0, \\ \sqrt{\frac{n+1}{\pi}} R_n^0(\rho), & \text{if m} = 0, \\ \sqrt{\frac{2(n+1)}{\pi}} R_n^m(\rho)\cos(m\varphi), & \text{if m} > 0, \end{cases}$$

with $R_n^{|m|}$ the radial Zernike polynomials [11]. The set Z_n^m is an orthonormal basis of the space of square integrable functions on the unit disk.

The values of the nonzero primary aberration coefficients are listed in Table 1. From the table it becomes clear that astigmatism is the dominant gap induced aberration. We see that for an air gap of only 25 nm the gap-induced aberrations are so severe that the focused spot is not even diffraction limited.

Table 1 *Nonzero primary aberration coefficients in unit λ (RMS): A_{20}= defocus, A_{22}=astigmatism and A_{40}=spherical aberration.*

	glass only	gap=0 nm	gap=25 nm	gap=50 nm	gap=75 nm
A_{20}	-0.0051	-0.0036	-0.0670	-0.0682	-0.0535
A_{22}	0.0000	0.0014	-0.0877	-0.1227	-0.1370
A_{40}	-0.0046	-0.0042	0.0127	0.0408	0.0625

We finally investigate to what extend the spot can be improved by compensating for the aberrations in the phase. Suppose that the phase $\widetilde{W}$ of the dominant electric field component E_x in the nominal focal plane $z=0$ vanishes while the amplitude of E_x is not corrected. In Fig. 19, the cross section of the normalized energy density of $|E_x|^2$ along the x-axis of the corrected spot for a gap of 25 nm is compared with that of the original spot for a gap of 25 nm and with that of the spot of zero gap. In Fig. 20 we show the same cross sections along the y-axis. The result suggests that, although the amplitude is not corrected for, it seems possible that a considerable improvement of the spot can be realized in this way.

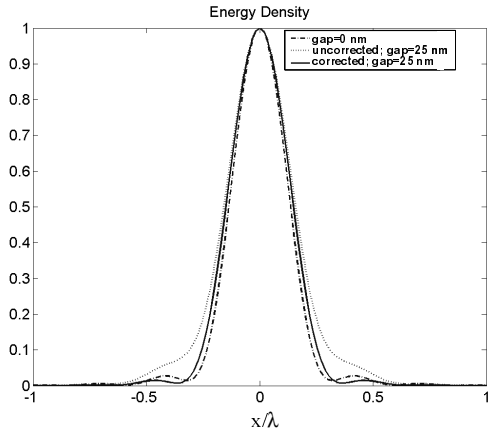

Figure 19 *Normalized cross sections along the x-axis of the energy density $|E_x|^2$ of the uncorrected and the phase corrected spot for an air gap of 25 nm, and the spot for zero gap.*

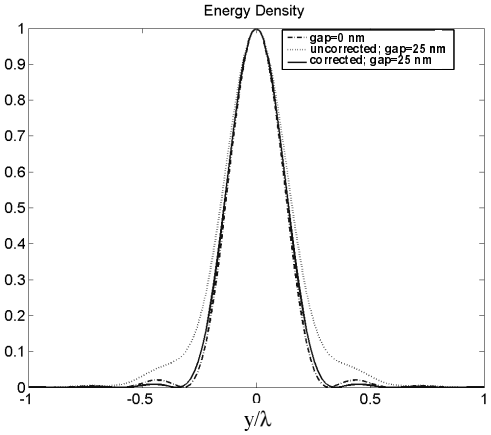

Figure 20 *Normalized cross sections along the y-axis of the energy density $|E_x|^2$ of the uncorrected and the phase corrected spot for an air gap of 25 nm, and the spot for zero gap.*

5. Proposal for a cover-layer incident, dual-layer near field system

A key strength of optical disk drives is the option to take the disk from the drive and exchange it. Because the data layer is buried under a transparent layer, the data is protected against small scratches resulting in a robust system. This does not seem feasible for a system with NA=1.9 because of the required refractive index n of the material that covers the data layer. This index n has to be larger than 1.9 to allow the marginal rays to propagate to the data layer and back to the SIL. Transparent materials with n > 1.9 are almost exclusively inorganic. These materials can be sputter deposited as thin layers but cannot be injection moulded or spin coated as thick layers, which would be required to make disks at low cost. If a cover-layer is not an option for NA=1.9 then neither is a spacer layer for multiple layer disks for this high NA. Therefore, disks for NA=1.9 will almost certainly have a single layer without

cover, which makes it more difficult to protect the data against for example SIL-disk collisions. Of course if a smaller NA were used then it would be possible to protect the data on the disks with a cover-layer. Transparent polymers with n≈1.7 that can be spin coated are available, so in principle a cover-layer for NA =1.5 is an option, but one that results in a smaller storage density per layer compared to NA =1.9. Note however that if a cover-layer is possible, then a spacer layer might also be feasible. This potentially enables cover-layer incident dual-layer recording with NA close to 1.5, which could result in a system that, compared to a NA=1.9 system, has better data protection, a larger storage capacity at a smaller density per layer, less complex mastering, a larger air gap and much larger lens making tolerances because a hemispherical rather than a super-hemispherical SIL can be used. Such a system does, however, require a lens that can jump focus from the top layer to the bottom layer, without a change of air gap and without significant extra aberrations. This concept is schematically depicted in Fig. 21 and 22.

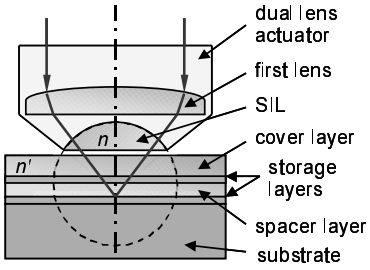

Figure 21 *Concept of near field read-out of the bottom layer of a dual-layer optical disk.*

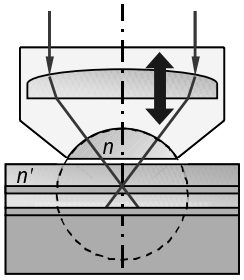

Figure 22 *Concept of near field read-out of the top layer of a dual-layer optical disk. Note the change in distance between the first lens element and the SIL.*

5.1 Spherical aberration in a dual-layer near field optical disk

To obtain more insight in the aberration compensation problem for a dual-layer near field optical recording system, we calculated the induced amount of spherical aberration per unit thickness of a spacer (or cover) layer for both far field and near field optical systems. For far field optics with relatively small NA there are well known approximations for these types of calculations based on paraxial optics. From these equations the rule of thumb is derived that the spherical aberration that is induced by focussing through a parallel plate scales with the fourth power of the NA. This is only accurate for low NA so we used exact analytical equations, without paraxial approximation, for our calculations for both the far field and the near field case. These equations were found to be in excellent agreement with results obtained with the lens design program Zemax. A full derivation of these equations is, unfortunately, beyond the scope of this paper so we limit ourselves to the numerical results. In Fig. 23 we show the RMS value in mλ/μm of the spherical aberration per micrometer thickness of a flat layer with refractive indices n=1.5, n=1.6 and n=1.7 for λ=405 nm. For NA < 1 we find that the spherical aberration is more or less independent of the refractive index and increases rapidly with NA. For low NA the curves follow the NA^4 rule of thumb. For

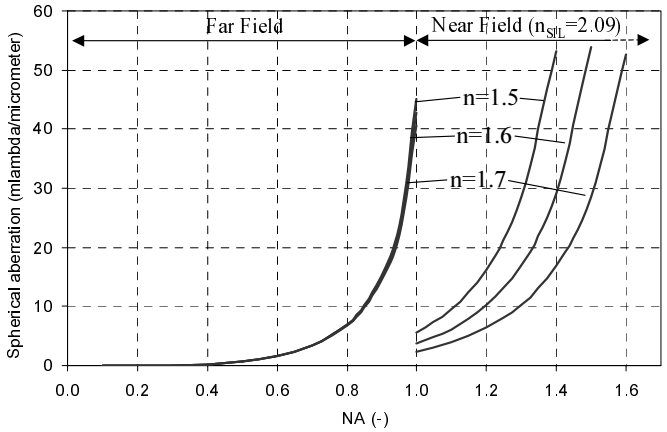

Figure 23 *Calculated spherical aberration per unit thickness induced by the focusing through a cover or spacer layer.*

high NA, but still smaller than 1, the rule of thumb significantly underestimates the amount of spherical aberration. Note that the value that is found for NA=0.85 and n=1.6 is 10 mλ/μm in accordance with Blu-ray Disc tolerances.
For near field with NA > 1 the spherical aberration was calculated with the assumption that the SIL is made of LaSF35 glass with n=2.09. From Fig. 23 it immediately becomes clear that the trend of the curves for NA < 1 is not continued into the near field regime of NA > 1. Instead, the curves are discontinuous due to the new geometry with the SIL on the interface with the flat layer. Note that there is a large dependence on the refractive index of the cover layer, with higher refractive index resulting in less spherical aberration. From Fig. 23 we see that the spherical aberration per micrometer thickness of a flat cover or spacer layer for NA=1.5 and n=1.7 is only three times larger than the value found for Blu-ray Disc. This is much less than one might, somewhat naively, expect based on the (in this case non-valid) NA^4 scaling rule of thumb. It thus turns out that, for a dual-layer NA=1.5 near field optical recording system, the amount of spherical aberration that must be corrected for while jumping focus from a first to a second layer is approximately 30 mλ/μm for a spacer layer with n=1.7. This leaves us the question what the minimum spacer layer thickness is that can be allowed in a dual-layer near field optical recording system. When we know this value it is possible to estimate whether or not a lens and light path can be designed that exactly compensates for the spherical aberration caused by the spacer layer.

5.2 Minimum spacer layer thickness in a dual-layer near field optical disk

We considered three generally accepted design rules for the minimum spacer layer thickness that apply to dual-layer optical disks such as dual-layer DVD and dual-layer Blu-ray Disc. These rules are

1. The spacer layer should have at least a thickness such that the focus error S-curves for both data layers are sufficiently separated for the focus servo controller to function.
2. Coherent cross talk between layers (interference of their mutual reflections on the detector) causes a modulation of the RF data signal. This effect should be sufficiently small to ensure that a slicer can follow the small fluctuations. Coherent cross talk decreases with increasing spacer thickness *h* because the amount of light from the out-of-focus layer on the detector decreases with increasing *h*
3. Incoherent cross talk from the data pattern on the out-of-focus layer should be sufficiently small. Incoherent noise is inversely proportional to the spot size and hence decreases with increasing *h*, because more data on the other layer is averaged due to the larger illuminated area for larger *h*.

Not all of the above applies to near field optical systems. For example our near field optical system does not rely on a focus error S curve but uses the GES to keep the distance between the lens and the disk constant. Furthermore, the second rule about coherent cross talk becomes irrelevant when the spacer layer thickness variation becomes smaller than approximately λ/4n. In that case the coherent cross talk is a constant, which has little influence on the performance of a bitdetector, even with a slicer. This means that when a spacer layer can be made with less than λ/4n thickness variation, the incoherent noise will determine the minimum spacer thickness. We estimated the minimum spacer layer thickness for a dual-layer near field system based on numbers for dual-layer DVD. As a reference we use the number $N_{<T>}$ of average run lengths <T> for the DVD channel code in the out of focus spot. We calculated this number for NA=0.6 and a 45 μm spacer thickness. If we keep this number constant and then calculate the minimum spacer thickness for a blue NA=1.5 system we find a minimum value of only h=1.3 μm. The fact that the cone of light for NA=1.5 is large and the relatively small average run length causes this number to be surprisingly small compared to the numbers for DVD and Blu-ray disk (see Table 2).

Table 2 *Spacer layer thickness scaling with incoherent noise.*

	λ (nm)	*NA*	<T> (nm)	$N_{<T>}$	*h* (μm)
DVD	660	0.60	640	2543	45
BD	405	0.85	248	12603	25
NF	405	1.50	140	2543	1.3

Previously we reported [7] on spincoated UV cured cover layers of a few micrometers thick with thickness variation of less than 30 nm. This implies that the coherent cross talk can indeed be made constant for the minimum spacer thickness at which the incoherent cross talk is still acceptable. Note also that the amount of spherical aberration that needs to be compensated while jumping from a first to a second layer for a few micrometer thick spacer layer in our NA=1.5 system is actually less than is the case for Blu-ray Disc with 25 micrometer spacer thickness: a 3 μm spacer times 30 mλ/μm for NA=1.5 or 25 μm spacer times 10 mλ/μm for NA=0.85. These result seems to confirm that a lens design with NA=1.5 for dual-layer disks can indeed be made.

5.3 Example of a lens design for cover layer incident near field read-out of a dual-layer optical disk

Here we present an example of a lens design for read-out of a dual-layer disk with a two-element NA =1.5 lens with manufacturing tolerances that are much larger than for our NA =1.9 design (Fig. 24). For example the SIL thickness tolerance for 15 mλ RMS spherical aberration is 12 μm, compared to only 0.2 μm for the NA=1.9 design. Our dual-layer near field lens design consists of a biaspherical lens with $NA_0 \approx 0.7$ and a hemispherical SIL made of BGO with n=2.21. The lens focuses aberration free through a 3 μm thick cover-layer with n=1.6 on both a top layer and a bottom layer. The n=1.6 spacer between the layers has a thickness of 3 μm. The focus jump is achieved with a change of the conjugate distance and a change of distance between the two lens elements. The distance between the lens elements can also be fixed if for example a liquid crystal spherical aberration compensating cell is used. This lens design example together with the considerations in the previous sections seems to confirm the feasibility of cover layer incident dual-layer near field disk systems with NA close to 1.5 and an ultimate storage capacity of approximately 300 GB on a double sided disk.

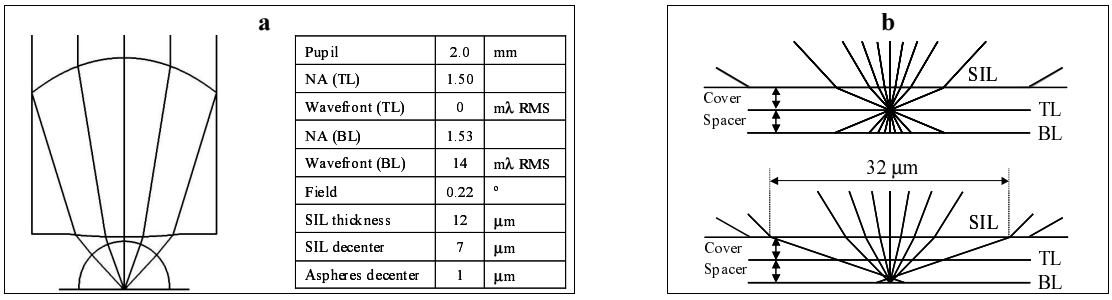

Figure 24 a) *NA=1.5 lens design and tolerances for a dual-layer cover-layer incident disk,* ***b)*** *schematic ray trace plot with NA=1.50 focus on the top layer (TL) and NA=1.53 focus on the bottom layer (BL).*

6. Conclusions

We have shown lens manufacturing results of our first-surface NA=1.9 lens. Typical lens aberrations are better than 40 mλ RMS. We have built a near field optical disk tester with a digital servo system. We have shown smooth servo pull-in without collision on the disk, and stable control of an air gap smaller than 30 nm. Furthermore we have shown read-out results of a 50 GB disk and we have shown that gap induced aberrations add significantly to other wave front aberrations that may be present in the system. Finally, we propose a cover-layer incident dual-layer near-field optical disk system with NA close to 1.5 and an ultimate storage capacity of approximately 300 GB on a double sided disk, the same as for a NA=1.9 first-surface disk system. We have started investigating which of the two options for near field optical recording has the largest chance of success.

Acknowledgement

The authors wish to thank Ir. L. Sander from Anteryon B.V., Messrs. C.L. Adema, P.W. de Haas and F.M.A. van Gaal from Philips Enabling Technologies Group and Mrs. Ing. M. Kaiser from Philips Research for their support with the design and manufacturing of the NA=1.9 lenses. We gratefully acknowledge M. Furuki and M. Shinoda from Sony Corporation for supplying a 50 GB ROM disk.

References

[1] Alexander Padiy et al., “Signal processing for 35 GB on a single-layer Blu-ray Disk”, submitted for presentation at ODS 2004

[2] A.H.J. Immink et al., “Adaptation and Timing Recovery for Two-Dimensional Optical Storage”, submitted for presentation at ODS 2004

[3] M. Shinoda et al., “High density near field readout over 100 GB capacity using solid immersion lens with NA of 2.05”, in SPIE Vol. 5069 Optical Data Storage 2003, edited by M. O’ Neill and N. Miyagawa, pp.306.

[4] T. Ishimoto et al., “Gap Servo System for a Biaxial Device Using an Optical Gap Signal in a Near Field Readout System,” Technical Digest ISOM/ODS 2002, pp. 287.

[5] M. Born and E. Wolf, “Principles of Optics”, 6th Ed. Pergamon Press, 1993, pp. 47.

[6] F. Zijp and Y.V. Martynov, “Static tester for characterization of optical near-field coupling phenomena”, in Optical Storage and Optical Information Processing, Han-Ping D. Shieh, Tom Milster, Editors, Proceedings of SPIE Vol. 4081, pp. 21-27 (2000)

[7] Y.V. Martynov et al.,”High-density first-surface magneto-optical recording using a blue laser, high numerical aperture objective and flying slider,” in Optical Data Storage 2001, Terril Hurst, Seiji Kobayashi, Editors, Proceedings of SPIE Vol. 4342, pp 209-212 (2002)

[8] J.S. Jo, T.D. Milster and J. K. Erwin, "Phase and amplitude apodization induced by focussing through an evanescent gap in a solid immersion lens microscope", Opt. Eng., 8, (2002), 1866-1875.

[9] V.S. Ignatowsky, Trans. Opt. Inst. Petrograd, Vol. I (1920), paper V.

[10] B. Richards and E. Wolf, "Electromagnetic diffraction in optical systems II. Structure of the image field in an aplanatic system", Proc. Roy. Soc. Lond. A, 253 (1959), 358-379.

[11] M. Born and E. Wolf, Prinicples of Optics, 7th Ed. p. 523, Cambridge University Press, 1999.